CHAPTER 3

# STUDY OF ONE DIMENSIONAL MHD NANOFLUID FLOW WITH HEAT AND MASS TRANSFER IN POROUS MEDIUM

SECTION I: STUDY OF WATER BASED NANOFLUID FLOW WITH HEAT AND MASS TRANSFER IN POROUS MEDIUM*

SECTION II: STUDY OF THERMAL RADIATION EFFECTS ON MHD CASSON NANOFLUID FLOW WITH HEAT AND MASS TRANSFER IN POROUS MEDIUM**

Content of this chapter is published in:

* Applied Thermal Engineering (Elsevier), 110 (2017) 864–874.

**Mathematics Today, 33 (2017) 99-120. ISSN 0976-3228.

# Chapter 3

## STUDY OF ONE DIMENSIONAL MHD NANOFLUID FLOW WITH HEAT AND MASS TRANSFER IN POROUS MEDIUM

Mass transfer is very important in the study of MHD as it cannot be neglected in many processes such as the dispersion of smoke from a chimney and home humidifier. Evaporation of alcohol from a beaker is an instance of mass transfer by natural convection. This chapter explores heat and mass transfer characteristics of one dimensional nanofluid flow through porous medium in presence of magnetic field.

This chapter is distributed in two sections. First section studies heat and mass transfer involved in water based nanofluid, whereas second section deals with Casson fluid based nanofluid flow taking effects of radiation in consideration.

## 3.1 SECTION I: STUDY OF WATER BASED NANOFLUID FLOW WITH HEAT AND MASS TRANSFER IN POROUS MEDIUM

The present section is concerned with the mathematical modelling of flow, heat and mass transfer in the unsteady natural convective magnetohydrodynamics flow of electrically conducting nanofluid, past over an oscillating vertical plate through porous medium. The features of the fluid flow, heat and mass transfer are analyzed by plotting graphs and the physical aspects are discussed in detail. Skin friction, Nusselt number and Sherwood number are derived with the help of velocity, temperature and concentration respectively. They are represented in tabular form.

### 3.1.1 Introduction of the problem

The study of magnetohydrodynamics flow considering heat and mass transfer has essential applications in physics, chemistry and engineering. One of the basic and important problems in this area is the hydromagnetic behavior of boundary layers along fixed or moving surfaces in presence of transverse magnetic field. MHD boundary layers are observed in various

technical systems employing liquid metal and plasma flow in presence of transverse magnetic field. Keeping this in view, Sheikholeslami et al. [84] investigated MHD free convection of $Al_2O_3$ – water nanofluid. MHD boundary layer flow and heat transfer of nanofluid past a vertical stretching sheet has been presented by Das et al. [10].

Heat transfer problems involving porous media have many engineering applications such as ground water pollution, geothermal energy recovery, flow through filtering media, thermal energy storage and crude oil extraction. Vadasz [114] explained heat and mass transfer in porous medium. Analytical investigation of MHD nanofluid flow in porous channel has been carried out by Sheikholeslami et al. [81].

Nanofluid flow in oscillating porous media rarely been a subject of thorough studies until the recent rise of marine applications in natural gas and oil processing. Oscillating vertical plates are used as heat exchangers in cooling systems. Currently, the industry of fossil-fuel offshore extraction and processing is increasingly interested on this particular class of flows.

### 3.1.2 Novelty of the problem

The aim of present investigation is to study the hydromagnetic gravity-driven convective boundary layer flow of nanofluid past an oscillating vertical plate in presence of uniform transverse magnetic field. The fluid flow is assumed to be induced due to the motion of the plate. The bounding plate has ramped temperature with ramped surface concentration and isothermal temperature with ramped surface concentration through porous medium. The governing equations are solved analytically. Obtained exact solutions are studied numerically and are elucidated with the help of graphs. Parametric study is performed for different parameters.

### 3.1.3 Mathematical formulation of the problem

Natural convective flow of nanofluid past an oscillating vertical plate is considered. Physical sketch of the problem is shown in Figure 3.1.1. Induced magnetic field by the fluid motion is negligible in comparison with the applied one as the magnetic Reynolds number is very small. Also, no external electric field is applied such that the effect of polarization of fluid is negligible. Hence, Reynolds number is also neglected. It is assumed that the effect of viscous dissipation and Ohmic dissipation are negligible in the energy equation and the level of species concentration is very low so, the Soret and Dufour effects are neglected. It is considered that porous medium has uniform geometry.

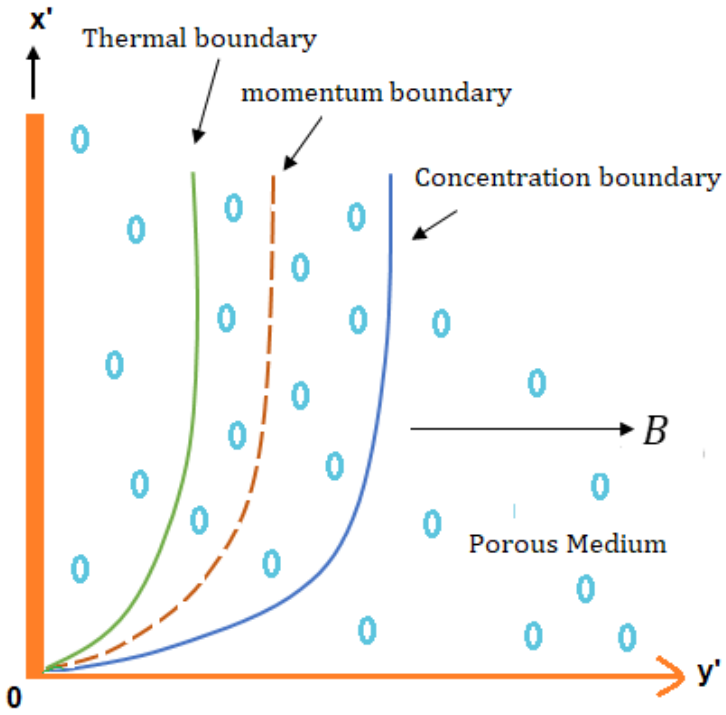


**Figure 3.1.1**: Physical sketch of the problem.

Initially, both fluid and the plate are at constant temperature $T_0$ and the concentration near the plate is assumed to be $C_0$. At time $t' > 0$, temperature of the wall is instantaneously raised and lowered to $T_0 + (T_w - T_0)\,{}^{t'}/_{t_0}$ when $t' \leq t_0$ and $T_w$ when $t' > t_0$. Concentration near

the plate is raised linearly to $C_0 + (C_w - C_0)\,{}^{t'}\!/_{t_0}$ when $t' \leq t_0$ and which is there after maintained constant $C_w$. The plate oscillates in its plane ($y' = 0$) according to equation $u' = u_0 sin(\omega' t')$ or $u_0 cos(\omega' t')$, $\omega'$ is the frequency of oscillation of the plate. The fluid is a water based nanofluid containing copper or silver as nanoparticles. It is further assumed that the base fluid and the suspended nanoparticles are in thermal equilibrium (by considering thermal equilibrium, particle-liquid mixture can be considered as conventional single phase fluid with properties of that are to be evaluated as functions of those of constituents [105]) and density is linearly dependent on buoyancy forces (Boussinesq approximation).

Under the above assumptions, the momentum, energy and mass transfer equations can be expressed as

$$\rho_{nf}\frac{\partial u'}{\partial t'} = \mu_{nf}\frac{\partial^2 u'}{\partial y'^2} - \sigma_{nf}B^2 u' - \frac{\mu_{nf}\varphi}{k_1}u' + g(\rho\beta)_{nf}(T' - T_0) + g(\rho\beta_C)_{nf}(C' - C_0), \quad (3.1.1)$$

$$\left(\rho c_p\right)_{nf}\frac{\partial T'}{\partial t'} = k_{nf}\frac{\partial^2 T'}{\partial y'^2}, \quad (3.1.2)$$

$$\frac{\partial C'}{\partial t'} = D\frac{\partial^2 C'}{\partial y'^2}, \quad (3.1.3)$$

where

$$\rho_{nf} = (1 - \emptyset)\rho_f + \emptyset\rho_s\,, \quad (3.1.4)$$

$$\mu_{nf} = \frac{\mu_f}{(1-\emptyset)^{2.5}}\,, \quad (3.1.5)$$

$$\sigma_{nf} = \sigma_f\left[1 + \frac{3(\sigma-1)\emptyset}{(\sigma+2)-(\sigma-1)\emptyset}\right], \quad (3.1.6)$$

$$\sigma = \frac{\sigma_s}{\sigma_f}\,, \quad (3.1.7)$$

$$(\rho\beta)_{nf} = (1 - \emptyset)(\rho\beta)_f + \emptyset(\rho\beta)_s\,, \quad (3.1.8)$$

$$k_{nf} = k_f[1 - 3\frac{\emptyset(k_f - k_s)}{2k_f + k_s + \emptyset(k_f - k_s)}], \quad (3.1.9)$$

$$(\rho c_p)_{nf} = (1 - \emptyset)(\rho c_p)_f + \emptyset(\rho c_p)_s\,, \quad (3.1.10)$$

$$u' = 0, \quad T' = T_0, \;\; C' = C_0; \; as \;\; y' \geq 0 \; and \;\; t' = 0 \quad (3.1.11)$$

$$u' = u_0 \sin(\omega' t') \; or \; u_0 \cos(\omega' t')\,,$$

$$T' = \begin{cases} T_0 + (T_w - T_0)\, {t'}/{t_0} \; if \;\; 0 < t' < t_0 \\ \quad T_w \qquad\qquad\qquad if \quad t' \geq t_0 \end{cases},$$

$$C' = \begin{cases} C_0 + (C_w - C_0)\, {t'}/{t_0} \; if \;\; 0 < t' < t_0 \\ \quad C_w \qquad\qquad\qquad if \quad t' \geq t_0 \end{cases}, \;\; as \;\; t' \geq 0 \; and \; y' = 0 \quad (3.1.12)$$

$$u' \to 0, T' \to T_0, \;\; C' \to C_0; \; as \;\; y' \to \infty \; and \; t' \geq 0 \quad (3.1.13)$$

Introducing non dimensional variables

$$y = \frac{u_0 y'}{v_f}, t = \frac{{u_0}^2 t'}{v_f}, u = \frac{u'}{u_0}, \theta = \frac{T' - T_0}{T_w - T_0}, C = \frac{C' - C_0}{C_w - C_0}, \omega = \frac{v_f \omega'}{{u_0}^2} \quad (3.1.14)$$

$$\frac{\partial u}{\partial t} = a_1 \frac{\partial^2 u}{\partial y^2} - \left(a_3 M + \frac{a_1}{k}\right) u + G_r a_2 \theta + G_m a_5 C \quad (3.1.15)$$

$$\frac{\partial \theta}{\partial t} = a_4 \frac{\partial^2 \theta}{\partial y^2} \quad (3.1.16)$$

$$\frac{\partial C}{\partial t} = \frac{1}{s_c} \frac{\partial^2 C}{\partial y^2} \quad (3.1.17)$$

with initial and boundary conditions

$$u = \theta = \; C = 0\,, \;\; y \geq 0, t = 0 \quad (3.1.18)$$

$$u = \sin(\omega' t') \text{ or } \cos(\omega' t')\,,$$

$$\theta = \begin{cases} t, & 0 < t \leq 1 \\ 1 & t > 1 \end{cases} = tH(t) - (t-1)H(t-1),$$

$$C = \begin{cases} t, & 0 < t \leq 1 \\ 1 & t > 1 \end{cases} = tH(t) - (t-1)H(t-1), \ y = 0, \ t > 0 \quad (3.1.19)$$

$$u \to 0, \theta \to 0, C \to 0 \quad as \ y \to \infty, t > 0 \quad (3.1.20)$$

where H (.) is Heaviside unit step function.

$$Pr = \frac{\mu_f \left(\rho c_p\right)_f}{\rho_f k_f}, \quad (3.1.21)$$

$$M = \frac{\sigma_f B^2 v_f}{\rho_f {u_0}^2}, \quad (3.1.22)$$

$$\frac{1}{k} = \frac{v_f \varphi^2}{k_1 {u_0}^2}, \quad (3.1.23)$$

$$Gr = \frac{v_f g \beta (T_w - T_0)}{{u_0}^3}, \quad (3.1.24)$$

$$\gamma = \frac{\mu_B \sqrt{2\pi_c}}{P_\gamma}, \quad (3.1.25)$$

$$Sc = \frac{v_f}{D}, \quad (3.1.26)$$

$$Gm = \frac{g \beta_c v_f (C_w - C_\infty)}{{u_0}^3}, \quad (3.1.27)$$

$$b_0 = 1 - \emptyset, \quad (3.1.28)$$

$$b_1 = (b_0 + \emptyset \frac{\rho_s}{\rho_f}), \quad (3.1.29)$$

$$b_2 = (b_0 + \emptyset \frac{(\rho\beta)_s}{(\rho\beta)_f}), \quad (3.1.30)$$

$$b_3 = (b_0 + \emptyset \frac{(\rho c_p)_s}{(\rho c_p)_f}), \quad (3.1.31)$$

$$b_4 = \frac{k_{nf}}{k_f}, \quad (3.1.32)$$

$$b_5 = \frac{\sigma_{nf}}{\sigma_f}, \tag{3.1.33}$$

$$b_6 = \frac{b_4}{b_3}, \tag{3.1.34}$$

$$b_7 = (b_0 + \emptyset \frac{(\rho\beta)_c}{(\rho\beta)_f}), \tag{3.1.35}$$

$$a_1 = \frac{1}{{b_0}^{2.5} b_1}, \tag{3.1.36}$$

$$a_2 = \frac{b_2}{b_1}, \tag{3.1.37}$$

$$a_3 = \frac{b_5}{b_1}, \tag{3.1.38}$$

$$a_4 = \frac{b_6}{Pr}, \tag{3.1.39}$$

$$a_5 = \frac{b_7}{b_1} \tag{3.1.40}$$

## 3.1.4 Solution of the problem

### 3.1.4.1 Solution for plate with ramped wall temperature

Taking Laplace transform of equations (3.1.15) to (3.1.17) with initial and boundary conditions (3.1.18) and (3.1.19).

$$\bar{\theta} = (1 - e^{-s}) F_8(y, s) \tag{3.1.41}$$

$$\bar{C} = F_{11}(y, s)(1 - e^{-s}) \tag{3.1.42}$$

$$\bar{u}_{sin}(y, s) = iG_1(y, s) + (1 - e^{-s}) H_1(y, s) \tag{3.1.43}$$

$$\bar{u}_{cos}(y, s) = G_1(y, s) + (1 - e^{-s}) H_1(y, s) \tag{3.1.44}$$

where

$$H_1(y, s) = G_2(y, s) - G_3(y, s) - G_4(y, s) \tag{3.1.45}$$

$$G_1(y,s) = \frac{1}{2}F_1(y,s) - \frac{1}{2}F_2(y,s) \quad (3.1.46)$$

$$G_2(y,s) = d_{17}F_3(y,s) + d_{18}F_4(y,s) + d_{12}F_5(y,s) + d_{15}F_6(y,s) \quad (3.1.47)$$

$$G_3(y,s) = d_{13}F_7(y,s) + d_{11}F_8(y,s) + d_{12}F_9(y,s) \quad (3.1.48)$$

$$G_4(y,s) = d_{16}F_{10}(y,s) + d_{14}F_{11}(y,s) + d_{15}F_{12}(y,s) \quad (3.1.49)$$

$$G_5(y,s) = d_{11}F_3(y,s) - d_{11}F_3(y,s) \quad (3.1.50)$$

$$G_6(y,s) = d_{16}F_3(y,s) + d_{14}F_4(y,s) + d_{15}F_6(y,s) \quad (3.1.51)$$

$$G_7(y,s) = d_{11}F_7(y,s) - d_{11}F_9(y,s) \quad (3.1.52)$$

$$F_1(y,s) = \frac{e^{-y\sqrt{\frac{s+d_2}{d_1}}}}{s+iw} \quad (3.1.53)$$

$$F_2(y,s) = \frac{e^{-y\sqrt{\frac{s+d_2}{d_1}}}}{s-iw} \quad (3.1.54)$$

$$F_3(y,s) = \frac{e^{-y\sqrt{\frac{s+d_2}{d_1}}}}{s} \quad (3.1.55)$$

$$F_4(y,s) = \frac{e^{-y\sqrt{\frac{s+d_2}{d_1}}}}{s^2} \quad (3.1.56)$$

$$F_5(y,s) = \frac{e^{-y\sqrt{\frac{s+d_2}{d_1}}}}{s-d_6} \quad (3.1.57)$$

$$F_6(y,s) = \frac{e^{-y\sqrt{\frac{s+d_2}{d_1}}}}{s-d_9} \quad (3.1.58)$$

$$F_7(y,s) = \frac{e^{-y\sqrt{s/a_4}}}{s} \quad (3.1.59)$$

$$F_8(y,s) = \frac{e^{-y\sqrt{s/a_4}}}{s^2} \tag{3.1.60}$$

$$F_9(y,s) = \frac{e^{-y\sqrt{s/a_4}}}{s-d_6} \tag{3.1.61}$$

$$F_{10}(y,s) = \frac{1}{s} e^{-y\sqrt{s_c\, s}} \tag{3.1.62}$$

$$F_{11}(y,s) = \frac{1}{s^2} e^{-y\sqrt{s_c\, s}} \tag{3.1.63}$$

$$F_{12}(y,s) = \frac{1}{s-d_9} e^{-y\sqrt{s_c\, s}} \tag{3.1.64}$$

Inverse Laplace transform of equation (3.1.41-3.1.44),

$$\theta(y,t) = f_8(y,t) - f_8(y,t-1)H(t-1) \tag{3.1.65}$$

$$C(y,t) = f_{11}(y,t) - f_{11}(y,t-1)H(t-1) \tag{3.1.66}$$

$$u_{sin}(y,t) = ig_1(y,t) + h_1(y,t-1)H(t-1) \tag{3.1.67}$$

$$u_{cos}(y,t) = g_1(y,t) + h_1(y,t-1)H(t-1) \tag{3.1.68}$$

### 3.1.4.2 Solution for plate with isothermal temperature

In this case, the initial and boundary conditions are same except Equation. (3.1.19), that becomes $\theta = 1\ at\ y = 0, t \geq 0$.

Now Laplace transform of equations (3.1.15) to (3.1.17) subject to new initial and boundary conditions will be

$$\bar{\theta} = F_7(y,s) \tag{3.1.69}$$

$$\bar{C} = F_{11}(y,s)(1-e^{-s}) \tag{3.1.70}$$

$$\bar{u}_{sin}(y,s) = iG_1(y,s) + G_5(y,s) + G_6(y,s)(1-e^{-s}) - G_7(y,s) - G_4(y,s)(1-e^{-s})$$

(3.1.71)

$$\bar{u}_{cos}(y,s) = G_1(y,s) + G_5(y,s) + G_6(y,s)(1-e^{-s}) - G_7(y,s) - G_4(y,s)(1-e^{-s})$$

(3.1.72)

Concentration will be same as given in equation (3.1.66) and expressions of temperature $\theta(y,t)$ and velocity $u(y,t)$ are given below.

$$\theta(y,t) = f_7(y,t) \tag{3.1.73}$$

$$u_{sin}(y,t) = ig_1(y,t) + g_5(y,t) + g_6(y,t) - g_6(y,t-1)H(t-1) - g_7(y,t) - g_4(y,t) + g_4(y,t-1)H(t-1) \tag{3.1.74}$$

$$u_{cos}(y,t) = g_1(y,t) + g_5(y,t) + g_6(y,t) - g_6(y,t-1)H(t-1) - g_7(y,t) - g_4(y,t) + g_4(y,t-1)H(t-1) \tag{3.1.75}$$

where

$$h_1(y,t) = g_2(y,t) - g_3(y,t) - g_4(y,t) \tag{3.1.76}$$

$$g_1(y,s) = \frac{1}{2}f_1(y,t) - \frac{1}{2}f_2(y,t) \tag{3.1.77}$$

$$g_2(y,t) = d_{17}f_3(y,t) + d_{18}f_4(y,t) + d_{12}f_5(y,t) + d_{15}f_6(y,t) \tag{3.1.78}$$

$$g_3(y,t) = d_{13}f_7(y,t) + d_{11}f_8(y,t) + d_{12}f_9(y,t) \tag{3.1.79}$$

$$g_4(y,t) = d_{16}f_{10}(y,t) + d_{14}f_{11}(y,t) + d_{15}f_{12}(y,t) \tag{3.1.80}$$

$$g_5(y,t) = d_{11}f_3(y,t) - d_{11}f_3(y,t) \tag{3.1.81}$$

$$g_6(y,t) = d_{16}f_3(y,t) + d_{14}f_4(y,t) + d_{15}f_6(y,t) \tag{3.1.82}$$

$$g_7(y,t) = d_{11}f_7(y,t) - d_{11}f_9(y,t) \tag{3.1.83}$$

$$f_1(y,t)=\frac{e^{-i\omega t}}{2}\left[e^{-y\sqrt{\frac{1}{d_1}(d_2-i\omega)}}\ erfc\ \left(\frac{y}{2\sqrt{d_1 t}}-\sqrt{(d_2-i\omega)t}\right)+e^{y\sqrt{\frac{1}{d_1}(d_2-i\omega)}}\ erfc\ \left(\frac{y}{2\sqrt{d_1 t}}+\sqrt{(d_2-i\omega)t}\right)\right] \tag{3.1.84}$$

$$f_2(y,t)=\frac{e^{i\omega t}}{2}\left[e^{-y\sqrt{\frac{1}{d_1}(d_2+i\omega)}}\ erfc\ \left(\frac{y}{2\sqrt{d_1 t}}-\sqrt{(d_2+i\omega)t}\right)+e^{y\sqrt{\frac{1}{d_1}(d_2+i\omega)}}\ erfc\ \left(\frac{y}{2\sqrt{d_1 t}}+\sqrt{(d_2+i\omega)t}\right)\right] \tag{3.1.85}$$

$$f_3(y,t)=\frac{1}{2}\left[e^{-y\sqrt{\frac{d_2}{d_1}}}\ erfc\ \left(\frac{y}{2\sqrt{d_1 t}}-\sqrt{d_2 t}\right)+e^{y\sqrt{\frac{d_2}{d_1}}}\ erfc\left(\frac{y}{2\sqrt{d_1 t}}+\sqrt{d_2 t}\right)\right] \tag{3.1.86}$$

$$f_4(y,t)=\frac{1}{2}\left[\left(t-\frac{y}{2\sqrt{d_2}d_1}\right)e^{-y\sqrt{\frac{d_2}{d_1}}}\ erfc\ \left(\frac{y}{2\sqrt{d_1 t}}-\sqrt{d_2 t}\right)+\left(t+\frac{y}{2\sqrt{d_2}d_1}\right)e^{y\sqrt{\frac{d_2}{d_1}}}\ erfc\ \left(\frac{y}{2\sqrt{d_1 t}}+\sqrt{d_2 t}\right)\right] \tag{3.1.87}$$

$$f_5(y,t)=\frac{e^{d_6 t}}{2}\left[e^{-y\sqrt{\frac{1}{d_1}(d_6+d_2)}}\ erfc\ \left(\frac{y}{2\sqrt{d_1 t}}-\sqrt{(d_6+d_2)t}\right)+e^{-y\sqrt{\frac{1}{d_1}(d_6+d_2)}}\ erfc\ \left(\frac{y}{2\sqrt{d_1 t}}+\sqrt{(d_6+d_2)t}\right)\right] \tag{3.1.88}$$

$$f_6(y,t)=\frac{e^{d_9 t}}{2}\left[e^{-y\sqrt{\frac{1}{d_1}(d_9+d_2)}}\ erfc\ \left(\frac{y}{2\sqrt{d_1 t}}-\sqrt{(d_9+d_2)t}\right)+e^{-y\sqrt{\frac{1}{d_1}(d_9+d_2)}}\ erfc\ \left(\frac{y}{2\sqrt{d_1 t}}+\sqrt{(d_9+d_2)t}\right)\right] \tag{3.1.89}$$

$$f_7(y,t)=erfc\ \left(\frac{y}{2\sqrt{a_4 t}}\right) \tag{3.1.90}$$

$$f_8(y,t)=\left(\frac{y^2}{2\,a_4}+t\right)erfc\ \left(\frac{y}{2\sqrt{a_4\,t}}\right)-\frac{y\sqrt{t}}{2\sqrt{a_4\,\pi}}e^{-\frac{y^2}{4ta_4}} \tag{3.1.91}$$

$$f_9(y,t)=\frac{e^{d_6 t}}{2}\left[e^{-y\sqrt{\frac{d_6}{a_4}}}\ erfc\ \left(\frac{y}{2\sqrt{a_4 t}}-\sqrt{d_6 t}\right)+e^{y\sqrt{\frac{d_6}{a_4}}}\ erfc\ \left(\frac{y}{2\sqrt{a_4 t}}+\sqrt{d_6 t}\right)\right] \tag{3.1.92}$$

$$f_{10}(y,t)=erfc\ \left(\frac{y\sqrt{Sc}}{2\sqrt{t}}\right) \tag{3.1.93}$$

$$f_{11}(y,t)=\left(\frac{y^2 Sc}{2}+t\right)erfc\ \left(\frac{y\sqrt{Sc}}{2\sqrt{t}}\right)-\frac{y\sqrt{\mathrm{Sc}\,t}}{2\sqrt{\pi}}e^{-\frac{y^2 Sc}{4t}} \tag{3.1.94}$$

$$f_{12}(y,t)=\frac{e^{d_9 t}}{2}\left[e^{-y\sqrt{Sc\,d_9}}\ erfc\ \left(\frac{y\sqrt{Sc}}{2\sqrt{t}}-\sqrt{d_9 t}\right)+e^{y\sqrt{Sc\,d_9}}\ erfc\ \left(\frac{y\sqrt{Sc}}{2\sqrt{t}}+\sqrt{d_9 t}\right)\right] \tag{3.1.95}$$

Here $u_{sin}(y,t)\ and\ u_{cos}(y,t)$ are the velocity profiles for sin and cosine oscillations respectively.

### 3.1.5 Nusselt Number

Using the equation (3.1.69), Nusselt number for Ramped wall temperature is

$$N_u = -[I_8(t) - I_8(t-1)H(t-1)] \tag{3.1.96}$$

Using the equation (3.1.73), Nusselt number for Isothermal temperature is

$$N_u = -[I_7(t)] \tag{3.1.97}$$

### 3.1.6 Sherwood Number

Using the equation (3.1.70), Sherwood Number is

$$s_h = -[I_{11}(t) - I_{11}(t-1)H(t-1)] \tag{3.1.98}$$

### 3.1.7 Skin Friction

Expressions of skin-friction for both cases are calculated from Equations (3.1.67-3.1.68) and (3.1.74 - 3.1.75).

#### 3.1.7.1 For ramped wall temperature

$$C_{f_{sin}}(y,t) = iI_{13}(t) + I_{20}(t) - I_{20}(t-1)H(t-1) \tag{3.1.99}$$

$$C_{f_{cos}}(y,t) = I_{13}(t) + I_{20}(t) - I_{20}(t-1)H(t-1) \tag{3.1.100}$$

#### 3.1.7.2 For isothermal temperature

$$C_{f_{sin}}(y,t) = iI_{13}(t) + I_{17}(t) + I_{18}(t) - I_{18}(t-1)H(t-1) - I_{19}(t) - I_{16}(t) + I_{16}(t-1)H(t-1)$$

(3.1.101)

$$C_{f_{cos}}(y,t) = I_{13}(t) + I_{17}(t) + I_{18}(t) - I_{18}(t-1)H(t-1) - I_{19}(t) - I_{16}(t) + I_{16}(t-1)H(t-1)$$

(3.1.102)

Where

$$I_{13}(y,s) = \frac{1}{2}I_1(t) - \frac{1}{2}I_2(t) \tag{3.1.103}$$

$$I_{14}(t) = d_{17}I_3(t) + d_{18}I_4(t) + d_{12}I_5(t) + d_{15}I_6(t) \tag{3.1.104}$$

$$I_{15}(t) = d_{13}I_7(t) + d_{11}I_8(t) + d_{12}I_9(t) \tag{3.1.105}$$

$$I_{16}(t) = d_{16}I_{10}(t) + d_{14}I_{11}(t) + d_{15}I_{12}(t) \tag{3.1.106}$$

$$I_{17}(t) = d_{11}I_3(t) - d_{11}I_3(t) \tag{3.1.107}$$

$$I_{18}(t) = d_{16}I_3(t) + d_{14}I_4(t) + d_{15}I_6(t) \tag{3.1.108}$$

$$I_{19}(t) = d_{11}I_7(t) - d_{11}I_9(t) \tag{3.1.109}$$

$$I_{20}(t) = I_{14}(t) - I_{15}(t) - I_{16}(t) \tag{3.1.110}$$

$$I_1(t) = e^{-i\omega t}\sqrt{\frac{d_2 - i\omega}{d_1}}\,\mathrm{erf}\left(\sqrt{(d_2 - i\omega)t}\right) + \frac{e^{-d_2 t}}{\sqrt{\pi d_1 t}} \tag{3.1.111}$$

$$I_2(t) = e^{i\omega t}\sqrt{\frac{d_2 + i\omega}{d_1}}\,\mathrm{erf}\left(\sqrt{(d_2 + i\omega)t}\right) + \frac{e^{-d_2 t}}{\sqrt{\pi d_1 t}} \tag{3.1.112}$$

$$I_3(t) = -\sqrt{\frac{d_2}{d_1}}\,\mathrm{erf}\left(\sqrt{d_2 t}\right) + \frac{e^{-d_2 t}}{\sqrt{\pi d_1 t}} \tag{3.1.113}$$

$$I_4(t) = -\frac{1}{\sqrt{4d_2 d_1}}\,\mathrm{erf}\left(\sqrt{d_2 t}\right) - t\sqrt{\frac{d_2}{d_1}}\,\mathrm{erf}\left(\sqrt{d_2 t}\right) + \sqrt{\frac{t}{\pi d_1}}\,e^{-d_2 t} \tag{3.1.114}$$

$$I_5(t) = e^{d_6 t}\sqrt{\frac{d_2 + d_6}{d_1}}\,\mathrm{erf}\left(\sqrt{(d_2 + d_6)t}\right) + \frac{e^{-d_2 t}}{\sqrt{\pi d_1 t}} \tag{3.1.115}$$

$$I_6(t) = e^{d_9 t}\sqrt{\frac{d_2 + d_9}{d_1}}\,\mathrm{erf}\left(\sqrt{(d_2 + d_9)t}\right) + \frac{e^{-d_2 t}}{\sqrt{\pi d_1 t}} \tag{3.1.116}$$

$$I_7(t) = \sqrt{\frac{1}{\pi a_4 t}} \tag{3.1.117}$$

$$I_8(t) = \frac{1}{2}\sqrt{\frac{t}{\pi a_4}} \tag{3.1.118}$$

$$I_9(t) = -e^{d_6 t}\sqrt{\frac{d_6}{a_4}}\,\mathrm{erf}\left(\sqrt{d_6 t}\right) + \sqrt{\frac{1}{\pi a_4 t}} \tag{3.1.119}$$

$$I_{10}(t) = \sqrt{\frac{Sc}{\pi t}} \tag{3.1.120}$$

$$I_{11}(t) = \frac{1}{2}\sqrt{\frac{tSc}{\pi}} \tag{3.1.121}$$

$$I_{12}(t) = -e^{d_9 t}\sqrt{Sc\ d_9}\,\mathrm{erf}\left(\sqrt{d_9 t}\right) + \sqrt{\frac{Sc}{\pi t}} \tag{3.1.122}$$

### 3.1.8 Results and Discussion

In this section, to get a clear insight on the physics of the problem, the obtained exact solutions are studied numerically and are elucidated with the help of graphs. Parametric study is performed for magnetic parameter $M$, Schimdt number $Sc$, permeability of porous medium $\kappa$, phase angle $\omega$, volume fraction parameter $\emptyset$ and time $t$ through Figures 3.1.2 to 3.1.8. Numerical values of skin-friction $C_f$, Nusselt number $Nu$ and Sherwood number $Sh$ are computed and presented in Tables 3.1.1 to 3.1.3 for different parameters.

Figure 3.1.2 displays the effect of nanoparticles volume fraction on nanofluid velocity. The nanofluid velocity decreases as volume fraction parameter increases. Since adding the particles leads to increase in dynamic viscosity and momentum diffusion of the fluid, it is clear that the thickness of the boundary layer decreases with increase in $\phi$.

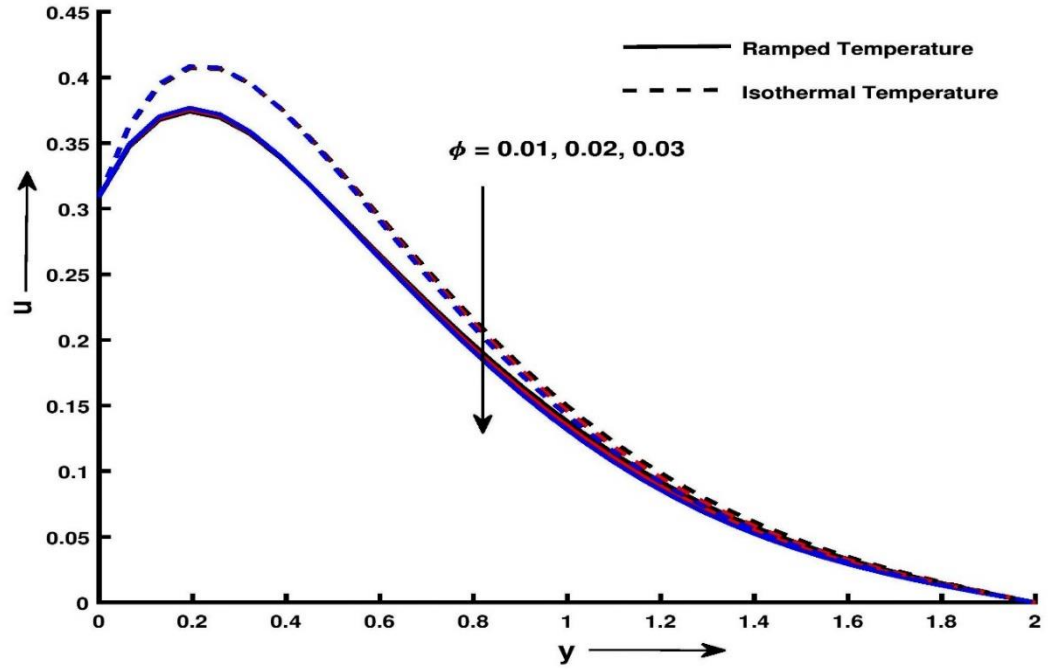


**Figure 3.1.2:** Velocity profile $u$ for $y$ and $\emptyset$ at $\omega = \pi, \mathrm{Pr} = 6.2, \mathrm{M} = 0.5,$ $\mathrm{Sc} = 0.66, \mathrm{Gm} = 5, \mathrm{Gr} = 10, \kappa = 0.4$ and $\mathrm{t} = 0.4$

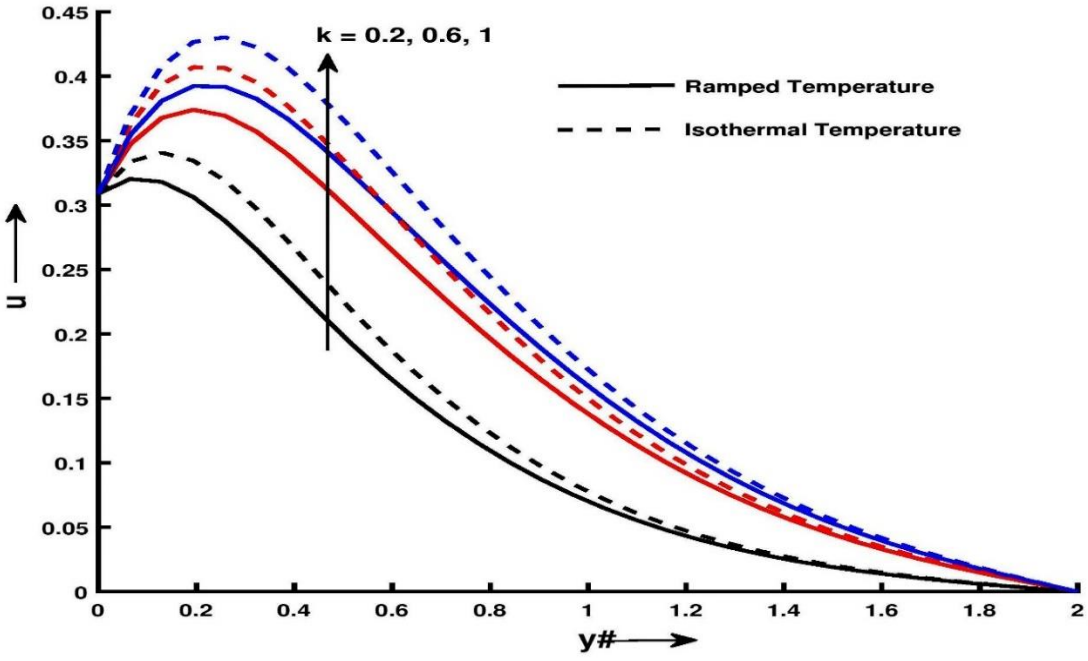


**Fig 3.1.3:** Velocity profile $u$ for $y$ and $\kappa$ at $\omega = \pi, \mathrm{Pr} = 6.2, \mathrm{M} = 0.5,$ $\mathrm{Sc} = 0.66, \mathrm{Gm} = 5, \mathrm{Gr} = 10, \emptyset = 0.03$ and $\mathrm{t} = 0.4$

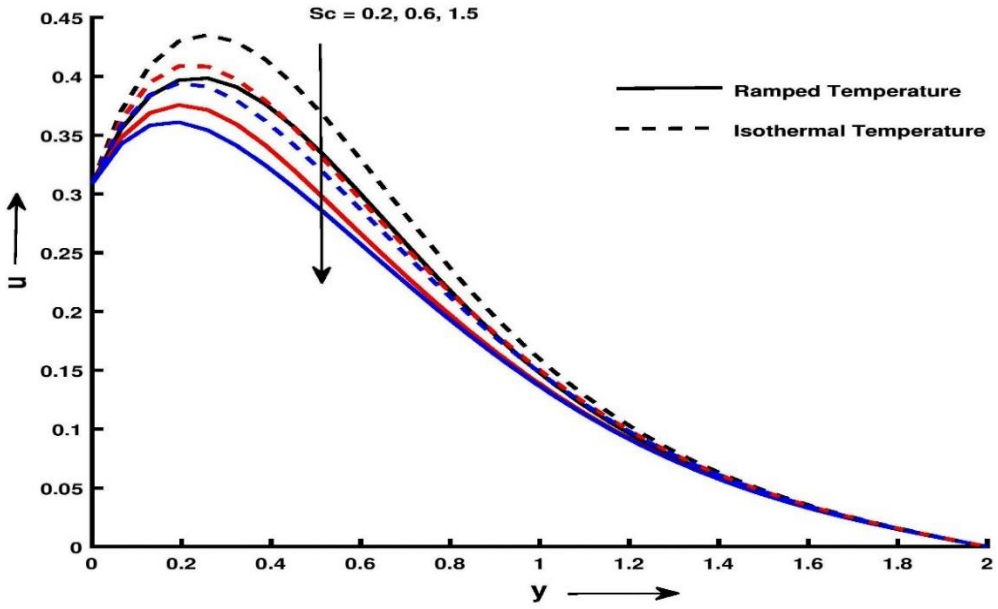


**Figure 3.1.4:** Velocity profile $u$ for $y$ and $Sc$ at $\omega = \pi, \mathrm{Pr} = 6.2, \mathrm{M} = 0.5,$ $\kappa = 0.4, \mathrm{Gm} = 5, \mathrm{Gr} = 10, \emptyset = 0.03$ and $\mathrm{t} = 0.4$

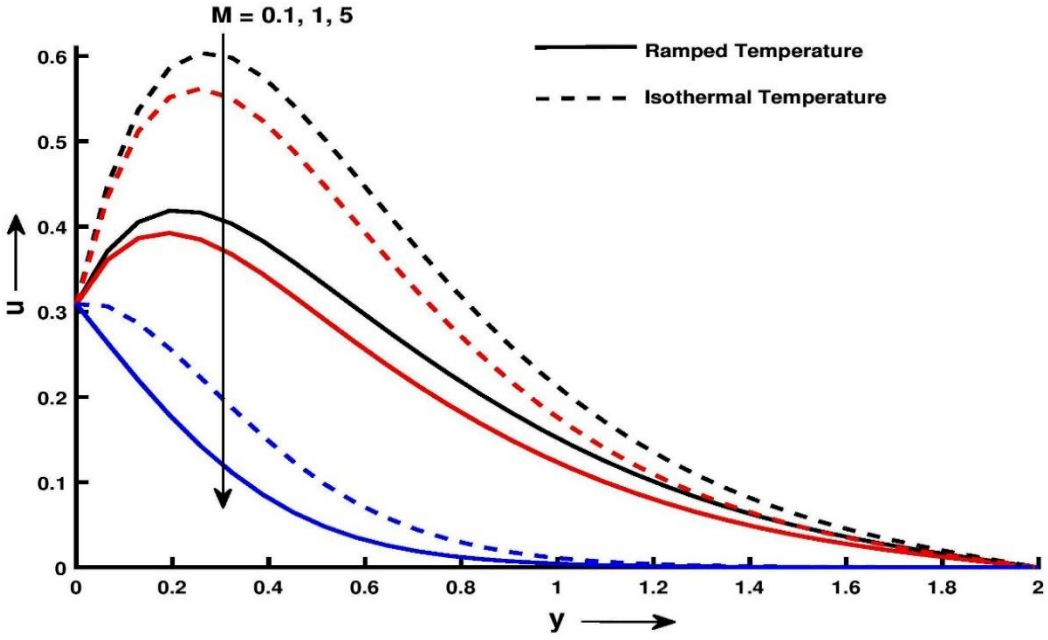


**Figure 3.1.5:** Velocity profile $u$ for $y$ and $M$ at $\omega = \pi, \mathrm{Gr} = 10, \mathrm{Pr} = 6.2,$ $\kappa = 0.4, \mathrm{Sc} = 0.66, \mathrm{Gm} = 5, \emptyset = 0.03$ and $\mathrm{t} = 0.4$

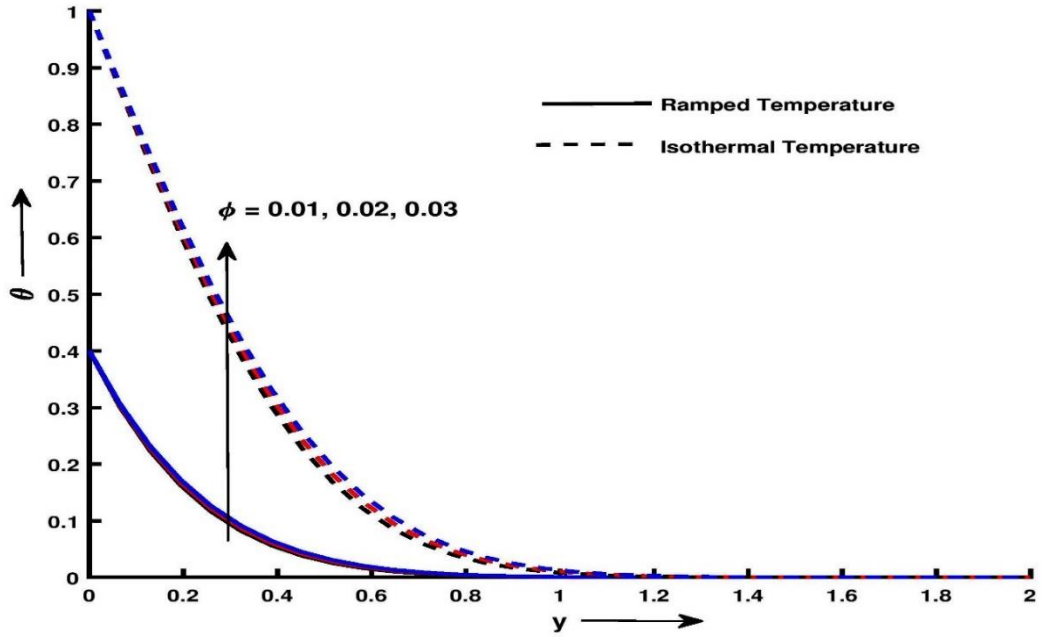


**Figure 3.1.6:** Temperature profile θ for $y$ and ∅ at $\omega = \pi, \mathrm{Gr} = 10, \mathrm{Pr} = 6.2,$ $\mathrm{M} = 0.5,\ \kappa = 0.4, \mathrm{Sc} = 0.66, \mathrm{Gm} = 5$ and $\mathrm{t} = 0.4$

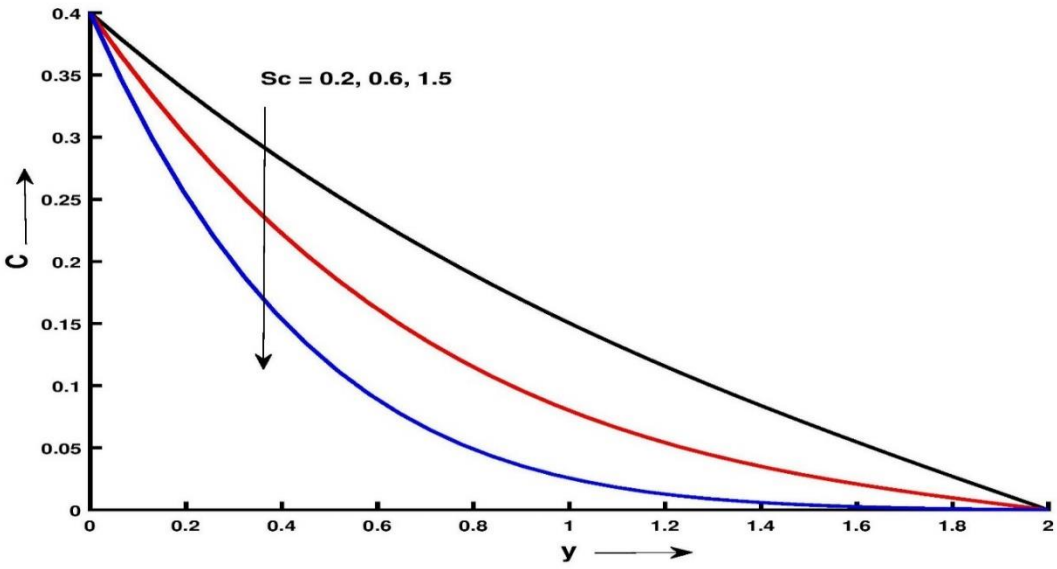


**Figure 3.1.7:** Concentration profile C for y and Sc at $\omega = \pi, \mathrm{Gr} = 10, \mathrm{Pr} = 6.2,$ $\mathrm{M} = 0.5,\ \kappa = 0.4,\ \mathrm{Gm} = 5, \emptyset = 0.03$ and $\mathrm{t} = 0.4$

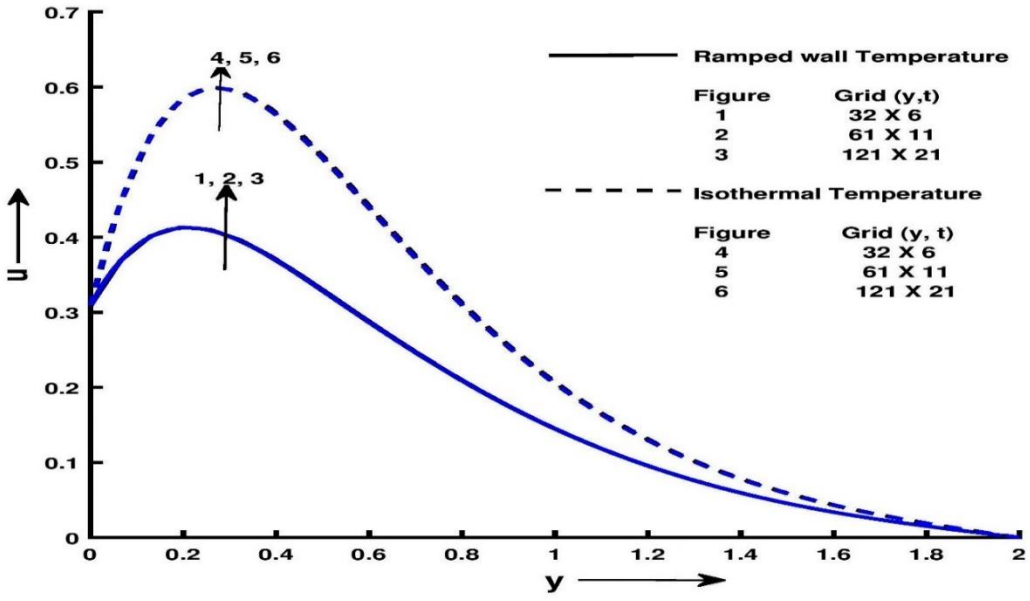


**Figure 3.1.8:** A graph showing the grid independency.

Figure 3.1.3 shows velocity profile for various values of permeability parameter $\kappa$ by keeping other parameters fixed. It is found that velocity increases with increase in $\kappa$. With increase in $\kappa$, the resistance of the porous medium decreases which increases the momentum of the flow regime, ultimately enhances the velocity field. Figure 3.1.4 depicts the effect of Schimdt number $Sc$ on the nanofluid velocity. It has been observed that the velocity decreases with an increase in the Schmidt number. Figure 3.1.5 reveals that the nanofluid velocity decreases for increasing values of magnetic parameter $M$. Physically, it is due to the transverse magnetic field resulting in resistive Lorentz force and upon increasing the values of $M$, this drag force increases, leading to the deceleration of the flow. Figure 3.1.6 exhibits the temperature profile for different values of volume fraction of nanoparticles, when the other parameters are fixed. It is observed that temperature of the nanofluid increases with increasing volume fraction of nanoparticles. Figure 3.1.7 exhibits the effect of thermo-diffusion on the species concentration for both ramped temperature and isothermal plates. It is evident from Figure 3.1.7 that, $C$ decreases on increasing $Sc$ throughout the boundary layer region. It is evident from Figure 3.1.8 that the results are independent of the grid size. The numerical values of

skin friction $C_f$ computed from the analytical expressions, are presented in Table 3.1.1. Tables 3.1.2 and 3.1.3 exhibit Nusselt number $Nu$ and Sherwood number $Sh$.

It is found from Table 3.1.1 that, for both ramped or isothermal temperature plates, skin friction $C_f$ reduces with the progress of time. The increased skin friction is generally a disadvantage in technical applications. It is observed that the skin friction due to the nanofluid flow decreases with an increase in either Grashof number $Gr$ or mass Grashof number $Gm$ or Schimdt number $Sc$ or permeability of porous medium $\kappa$**.** Consequently, the hot nanofluid near the plate surface is carried away quickly as Grashof number $Gr$ increases. Therefore, the skin friction at the plate reduces. It is observed from Table 3.1.2 that, Nusselt number $Nu$ decreases on increasing $t$ for ramped temperature and otherwise for isothermal case. Table 3.1.3 shows that, Sherwood number $Sh$ decreases with increase in $t$ or Schimdt number $Sc$ for both ramped temperature and isothermal plates.

**Table 3.1.1:** Skin friction variation

| $\emptyset$ | $Pr$ | $M$ | $Sc$ | $Gr$ | $Gm$ | $\kappa$ | $t$ | $C_f$ for Ramped temperature | $C_f$ for isothermal temperature |
|---|---|---|---|---|---|---|---|---|---|
| 0.05 | 5 | 0.5 | 1.5 | 10 | 5 | 0.6 | 0.4 | -10.0413 | -3.7254 |
| 0.1 | 5 | 0.5 | 1.5 | 10 | 5 | 0.6 | 0.4 | -7.0138 | -3.0141 |
| 0.15 | 5 | 0.5 | 1.5 | 10 | 5 | 0.6 | 0.4 | -5.3196 | -2.6330 |
| 0.15 | 6 | 0.5 | 1.5 | 10 | 5 | 0.6 | 0.4 | -5.8340 | -2.5817 |
| 0.15 | 7 | 0.5 | 1.5 | 10 | 5 | 0.6 | 0.4 | -6.3083 | -2.5390 |
| 0.15 | 5 | 0.6 | 1.5 | 10 | 5 | 0.6 | 0.4 | -5.0336 | -2.5646 |
| 0.15 | 5 | 0.7 | 1.5 | 10 | 5 | 0.6 | 0.4 | -4.7467 | -2.4943 |

| | | | | | | | | | |
|---|---|---|---|---|---|---|---|---|---|
| 0.15 | 5 | 0.5 | 2 | 10 | 5 | 0.6 | 0.4 | -5.7819 | -3.0954 |
| 0.15 | 5 | 0.5 | 2.5 | 10 | 5 | 0.6 | 0.4 | -6.1914 | -3.5048 |
| 0.15 | 5 | 0.5 | 1.5 | 11 | 5 | 0.6 | 0.4 | -5.6877 | -2.7324 |
| 0.15 | 5 | 0.5 | 1.5 | 12 | 5 | 0.6 | 0.4 | -6.0557 | -2.8318 |
| 0.15 | 5 | 0.5 | 1.5 | 10 | 6 | 0.6 | 0.4 | -5.6474 | -2.9608 |
| 0.15 | 5 | 0.5 | 1.5 | 10 | 7 | 0.6 | 0.4 | -5.9751 | -3.2885 |
| 0.15 | 5 | 0.5 | 1.5 | 10 | 5 | 0.7 | 0.4 | -5.5890 | -2.6963 |
| 0.15 | 5 | 0.5 | 1.5 | 10 | 5 | 0.8 | 0.4 | -5.8455 | -2.7557 |
| 0.15 | 5 | 0.5 | 1.5 | 10 | 5 | 0.6 | 0.5 | -6.4490 | -3.1649 |
| 0.15 | 5 | 0.5 | 1.5 | 10 | 5 | 0.6 | 0.6 | -7.5796 | -3.6939 |

**Table 3.1.2:** Nusselt number variation

| $\emptyset$ | $Pr$ | $t$ | $Nu$ for Ramped Temperature | $Nu$ for isothermal Temperature |
|---|---|---|---|---|
| 0.05 | 5 | 0.4 | -0.3692 | -1.8462 |
| 0.1 | 5 | 0.4 | -0.3427 | -1.7134 |
| 0.15 | 5 | 0.4 | -0.3186 | -1.5932 |
| 0.15 | 6 | 0.4 | -0.3490 | -1.7452 |
| 0.15 | 7 | 0.4 | -0.3770 | -1.8850 |
| 0.15 | 5 | 0.5 | -0.3562 | -1.4250 |
| 0.15 | 5 | 0.6 | -0.3902 | -1.3008 |

**Table 3.1.3:** Sherwood Number variation

| $Sc$ | $t$ | Sherwood Number $Sh$ |
|---|---|---|
| 1.5 | 0.4 | -0.2185 |
| 2.0 | 0.4 | -0.2523 |
| 2.5 | 0.4 | -0.2821 |
| 1.5 | 0.5 | -0.2443 |
| 1.5 | 0.6 | -0.2676 |

## 3.1.9 Conclusion

Key findings of this section are summarized as follows

- Nanofluid velocity decreases with increase in magnetic parameter $M$ and Schimdt number $Sc$.
- Nanofluid velocity is more for isothermal temperature as compared to ramped plate.
- Concentration decreases with increase in Schimdt number $Sc$.
- Nusselt number $Nu$ decreases on increasing $t$ for ramped temperature and otherwise for isothermal case.
- Sherwood number $Sh$ decreases with increase in $t$ or Schimdt number $Sc$ for both ramped temperature and isothermal plates.
- Nanofluid velocity decreases with increase in volume fraction parameter $\emptyset$.
- Skin friction and Nusselt number increases with increase in volume fraction parameter $\emptyset$.

## 3.2 SECTION II: STUDY OF THERMAL RADIATION EFFECTS ON MHD CASSON NANOFLUID FLOW WITH HEAT AND MASS TRANSFER IN POROUS MEDIUM

Present investigation is concerned with natural convective flow of Casson nanofluid past an oscillating vertical plate with ramped or isothermal wall temperature in presence of magnetic field and radiation. Fluid passes through a porous medium.

### 3.2.1 Introduction of the problem

A distinctive nanofluid namely Casson nanofluid which is ideal to fit rheological data for fluids like blood. Such fluids behaves as solid when yield stress is more than the shear stress, and it starts to deform when yield stress becomes lesser than shear stress. This study has number of applications in polymer extrusion, paper production, glass blowing, paint production, aerodynamic extrusion of plastic sheet, crude oil and food industries including chocolate, honey, mayonnaise production etc. Usman et al. [113] investigated Casson nanofluid with heat and mass transfer in presence of magnetic field. Casson MHD nanofluid flow past horizontal stretching was studied by Kamram et al. [27].

Thermal radiation effects have significant uses in space technology and heat transfer processes in polymer processing industry as the quality of the product depends on the heat controlling factors. Thus investigation of thermal radiation effects on Casson nanofluid flow can be a boon in polymer and crude oil industries. Oyelakin et al. [55] discussed effects of thermal radiations on unsteady Casson nanofluid flow.

### 3.2.2 Novelty of the problem

Velocity, temperature and concentration profiles associative with natural convective boundary layer MHD flow of Casson nanofluid past an oscillating vertical plate in presence

of a uniform transverse magnetic field with ramped wall temperature are analyzed. This investigation may find applications in magnetic nanomaterial processing and cooling processes in industries and reactors.

### 3.2.3 Mathematical Formulation of the Problem

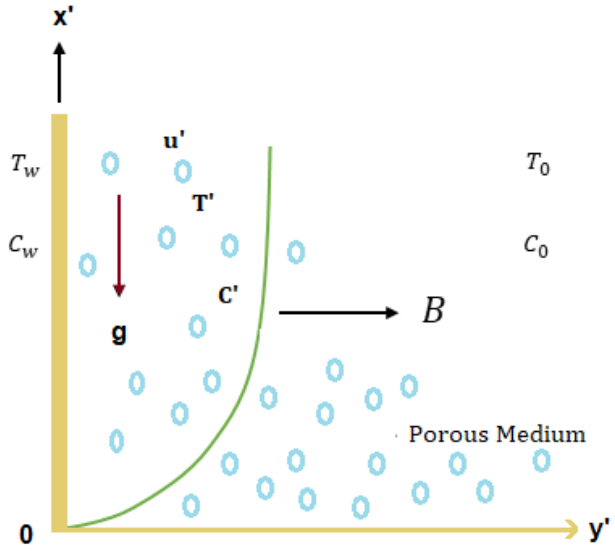


**Figure 3.2.1**: Physical sketch of the problem.

Unsteady MHD flow of non-Newtonian electrically conducting Casson nanofluid near an infinite vertical plate with ramped wall temperature in porous medium is considered. As shown in Figure 3.2.1, $x$ axis is along the wall in the upward direction and $y'$ axis is normal to it. A uniform transverse magnetic field $B$ is applied in $y'$ direction. Initially, temperature and concentration near the plate is assumed to be $T_0$ and $C_0$ respectively. Temperature of the wall is $T_0 + (T_w - T_0)\,{}^{t'}/_{t_0}$ when $0 < t' \leq t_0$ and $T_w$ for $t' > t_0$. Similarly, concentration near the plate is $C_0 + (C_w - C_0)\,{}^{t'}/_{t_0}$ for $0 < t' \leq t_0$ and $C_w$ when $t' > t_0$. Effects of

viscous dissipation, Ohmic dissipation, induced magnetic and electric fields are neglected. Nanofluid under consideration is assumed to be single phase.

Under above assumptions, governing equations are given below:

$$\rho_{nf}\frac{\partial u'}{\partial t'} = \mu_{nf}\left(1+\frac{1}{\gamma}\right)\frac{\partial^2 u'}{\partial y'^2} - \sigma_{nf}B^2u' - \frac{\mu_{nf}\varphi}{k_1}u' + g(\rho\beta)_{nf}(T'-T_0) + g(\rho\beta_C)_{nf}(C'-C_0), \tag{3.2.1}$$

$$\left(\rho c_p\right)_{nf}\frac{\partial T'}{\partial t'} = k_{nf}\frac{\partial^2 T'}{\partial y'^2} - \frac{\partial q_r}{\partial y'}, \tag{3.2.2}$$

$$\frac{\partial C'}{\partial t'} = D\frac{\partial^2 C'}{\partial y'^2}, \tag{3.2.3}$$

where

$$\rho_{nf} = (1-\emptyset)\rho_f + \emptyset\rho_s, \tag{3.2.4}$$

$$\mu_{nf} = \frac{\mu_f}{(1-\emptyset)^{2.5}}, \tag{3.2.5}$$

$$\sigma_{nf} = \sigma_f\left[1+\frac{3(\sigma-1)\emptyset}{(\sigma+2)-(\sigma-1)\emptyset}\right], \sigma = \frac{\sigma_s}{\sigma_f}, \tag{3.2.6}$$

$$(\rho\beta)_{nf} = (1-\emptyset)(\rho\beta)_f + \emptyset(\rho\beta)_s, \tag{3.2.7}$$

$$k_{nf} = k_f\left[1-3\frac{\emptyset(k_f-k_s)}{2k_f+k_s+\emptyset(k_f-k_s)}\right], \tag{3.2.8}$$

$$\left(\rho c_p\right)_{nf} = (1-\emptyset)(\rho c_p)_f + \emptyset(\rho c_p)_s, \tag{3.2.9}$$

$$q_r = -\frac{4\sigma^*}{3k^*}\frac{\partial T'^4}{\partial y'}. \tag{3.2.10}$$

Considering Rosseland approximation [61],

$$q_r = -\frac{4\sigma^*}{3k^*}\frac{\partial\left(4T_0{}^3T'-3T_0{}^4\right)}{\partial y'}. \tag{3.2.11}$$

Using this $q_r$ in (3.2.2):

$$\left(\rho c_p\right)_{nf}\frac{\partial T'}{\partial t'} = (k_{nf} + \frac{16\sigma^* {T_0}^3}{3k^*})\frac{\partial^2 T'}{\partial {y'}^2}. \tag{3.2.12}$$

Initial and boundary conditions are

$$u' = 0, \quad T' = T_0, \ \ C' = C_0; \ as \ \ y' \geq 0 \ and \ \ t' < 0, \tag{3.2.13}$$

$u' = u_0 \sin(\omega' t')\ or\ u_0 \cos(\omega' t')$ ,

$$T' = \begin{cases} T_0 + (T_w - T_0)\, {t'}/{t_0}\ if & 0 < t' < t_0 \\ T_w \qquad\qquad\quad if & t' \geq t_0 \end{cases},$$

$$C' = \begin{cases} C_0 + (C_w - C_0)\, {t'}/{t_0}\ if & 0 < t' < t_0 \\ C_w \qquad\qquad\quad if & t' \geq t_0 \end{cases}, \ \ as \ \ t' \geq 0 \ and \ y' = 0; \tag{3.2.14}$$

$$u' \to 0, T' \to T_0, \ \ C' \to C_0; \ as \ \ y' \to \infty \ and \ t' \geq 0. \tag{3.2.15}$$

Introducing non dimensional variables

$$y = \frac{u_0 y'}{v_f}, t = \frac{{u_0}^2 t'}{v_f}, u = \frac{u'}{u_0}, \theta = \frac{T' - T_0}{T_w - T_0}, C = \frac{C' - C_0}{C_w - C_0}, \omega = \frac{v_f \omega'}{{u_0}^2}, \tag{3.2.16}$$

Equations (3.2.1), (3.2.2) and (3.2.3) become

$$\frac{\partial u}{\partial t} = \left(1 + \frac{1}{\gamma}\right) a_1 \frac{\partial^2 u}{\partial y^2} - \left(a_3 M + \frac{a_1}{k}\right) u + G_r a_2 \theta + G_m a_5 C, \tag{3.2.17}$$

$$\frac{\partial \theta}{\partial t} = a_4 \frac{\partial^2 \theta}{\partial y^2}, \tag{3.2.18}$$

$$\frac{\partial C}{\partial t} = \frac{1}{S_c}\frac{\partial^2 C}{\partial y^2}, \tag{3.2.19}$$

with initial and boundary conditions

$$u = \theta = \ C = 0\,, \qquad y \geq 0, t = 0, \tag{3.2.20}$$

$u = \sin(wt)\ or\ \cos(wt),$

$\theta = \begin{cases} t, & 0 < t \leq 1 \\ 1 & t > 1 \end{cases} = tH(t) - (t-1)H(t-1),$

$C = t,\ \ y = 0,\ \ t > 0;$ (3.2.21)

$u \to 0, \theta \to 0, C \to 0 \quad as\ \ y \to \infty, t > 0;$ (3.2.22)

where

H (.) is Heaviside unit step function,

$b_0 = 1 - \emptyset,$ (3.2.23)

$b_1 = \left(b_0 + \emptyset \frac{\rho_s}{\rho_f}\right),$ (3.2.24)

$b_2 = \left(b_0 + \emptyset \frac{(\rho\beta)_s}{(\rho\beta)_f}\right),$ (3.2.25)

$b_3 = \left(b_0 + \emptyset \frac{(\rho c_p)_s}{(\rho c_p)_f}\right),$ (3.2.26)

$b_4 = \frac{k_{nf}}{k_f},$ (3.2.27)

$b_5 = \frac{\sigma_{nf}}{\sigma_f},$ (3.2.28)

$b_6 = \frac{b_4}{b_3},$ (3.2.29)

$b_7 = \left(b_0 + \emptyset \frac{(\rho\beta)_c}{(\rho\beta)_f}\right),$ (3.2.30)

$a_1 = \frac{1}{{b_0}^{2.5} b_1},$ (3.2.31)

$a_2 = \frac{b_2}{b_1},$ (3.2.32)

$$a_3 = \frac{b_5}{b_1}, \tag{3.2.33}$$

$$a_4 = \frac{b_4 + Nr}{b_3 Pr}, \tag{3.2.34}$$

$$a_5 = \frac{b_7}{b_1}, \tag{3.2.35}$$

$$Pr = \frac{\mu_f \left(\rho c_p\right)_f}{\rho_f k_f}, \tag{3.2.36}$$

$$M = \frac{\sigma_f B^2 v_f}{\rho_f {u_0}^2}, \tag{3.2.37}$$

$$\frac{1}{k} = \frac{v_f \varphi^2}{k_1 {u_0}^2}, \tag{3.2.38}$$

$$Gr = \frac{v_f g \beta (T_w - T_0)}{{u_0}^3}, \tag{3.2.39}$$

$$\gamma = \frac{\mu_B \sqrt{2\pi_c}}{P_\gamma}, \tag{3.2.40}$$

$$Sc = \frac{v_f}{D}, \tag{3.2.41}$$

$$Gm = \frac{g \beta_c v_f (C_w - C_0)}{{u_0}^3}, \tag{3.2.42}$$

$$Nr = \frac{16 \sigma^* {T_0}^3}{3 k^* k_f}. \tag{3.2.43}$$

## 3.2.4 Solution of the Problem

Taking Laplace transform of equations (3.2.17) – (3.2.19) with initial and boundary conditions (3.2.20) – (3.2.22)

$$\bar{\theta} = (1 - e^{-s}) F_8(y, s), \tag{3.2.44}$$

$$\bar{C} = F_{11}(y, s), \tag{3.2.45}$$

$$\bar{u}_{sin}(y,s) = \frac{i}{2}F_1(y,s) - \frac{i}{2}F_2(y,s) + (1-e^{-s})G_1(y,s) + G_2(y,s) - (1-e^{-s})G_3(y,s) - G_4(y,s), \quad (3.2.46)$$

$$\bar{u}_{cos}(y,s) = \frac{1}{2}F_1(y,s) + \frac{1}{2}F_2(y,s) + (1-e^{-s})G_1(y,s) + G_2(y,s) - (1-e^{-s})G_3(y,s) - G_4(y,s), \quad (3.2.47)$$

where

$$F_1(y,s) = \frac{e^{-y\sqrt{\frac{s+d_2}{d_1}}}}{s+iw}, \quad (3.2.48)$$

$$F_2(y,s) = \frac{e^{-y\sqrt{\frac{s+d_2}{d_1}}}}{s-iw}, \quad (3.2.49)$$

$$G_1(y,s) = d_{13}F_3(y,s) + d_{11}F_4(y,s) + d_{12}F_5(y,s), \quad (3.2.50)$$

$$G_2(y,s) = d_{16}F_3(y,s) + d_{14}F_4(y,s) + d_{15}F_6(y,s), \quad (3.2.51)$$

$$G_3(y,s) = d_{13}F_7(y,s) + d_{11}F_8(y,s) + d_{12}F_9(y,s), \quad (3.2.52)$$

$$G_4(y,s) = d_{16}F_{10}(y,s) + d_{14}F_{11}(y,s) + d_{15}F_{12}(y,s), \quad (3.2.53)$$

$$F_3(y,s) = \frac{e^{-y\sqrt{\frac{s+d_2}{d_1}}}}{s}, \quad (3.2.54)$$

$$F_4(y,s) = \frac{e^{-y\sqrt{\frac{s+d_2}{d_1}}}}{s^2}, \quad (3.2.55)$$

$$F_5(y,s) = \frac{e^{-y\sqrt{\frac{s+d_2}{d_1}}}}{s-d_6}, \quad (3.2.56)$$

$$F_6(y,s) = \frac{e^{-y\sqrt{\frac{s+d_2}{d_1}}}}{s-d_9}, \quad (3.2.57)$$

$$F_7(y,s) = \frac{e^{-y\sqrt{s/a_4}}}{s}, \tag{3.2.58}$$

$$F_8(y,s) = \frac{e^{-y\sqrt{s/a_4}}}{s^2}, \tag{3.2.59}$$

$$F_9(y,s) = \frac{e^{-y\sqrt{s/a_4}}}{s-d_6}, \tag{3.2.60}$$

$$F_{10}(y,s) = \frac{1}{s}e^{-y\sqrt{s_c\, s}}, \tag{3.2.61}$$

$$F_{11}(y,s) = \frac{1}{s^2}e^{-y\sqrt{s_c\, s}}, \tag{3.2.62}$$

$$F_{12}(y,s) = \frac{1}{s-d_9}e^{-y\sqrt{s_c\, s}}. \tag{3.2.63}$$

Inverse Laplace transform of equations (3.2.44) – (3.2.47), give rise to following solutions.

### 3.2.4.1 Solutions for Plate with Ramped Wall Temperature

$$\theta(y,t) = f_8(y,t) - f_8(y,t-1)H(t-1), \tag{3.2.64}$$

$$C(y,t) = f_{11}(y,t), \tag{3.2.65}$$

$$u_{sin}(y,t) = \frac{i}{2}f_1(y,t) - \frac{i}{2}f_2(y,t) + g_1(y,t) - g_1(y,t-1)H(t-1) + g_2(y,t) - g_3(y,t) + g_3(y,t-1)\ H(t-1) - g_4(y,t), \tag{3.2.66}$$

$$u_{cos}(y,t) = \frac{1}{2}f_1(y,t) - \frac{1}{2}f_2(y,t) + g_1(y,t) - g_1(y,t-1)H(t-1) + g_2(y,t) - g_3(y,t) + g_3(y,t-1)\ H(t-1) - g_4(y,t). \tag{3.2.67}$$

### 3.2.4.2 Solutions for Plate with Constant Temperature

Here the initial and boundary conditions are the same except Eq. (3.2.21), which is

$$\theta = 1\ at\ y = 0, t \geq 0. \tag{3.2.68}$$

Concentration will be same as given in equation (3.2.65) and expressions of temperature $\theta(y,t)$ and velocity $u(y,t)$ are given below. (Similar steps as in section 3.1)

$$\theta(y,t) = f_7(y,t), \tag{3.2.69}$$

$$u_{sin}(y,t) = \frac{i}{2}f_1(y,t) - \frac{i}{2}f_2(y,t) + (d_{11}+d_{16})f_3(y,t) + d_{14}f_4(y,t) - d_{11}f_5(y,t) + d_{15}f_6(y,t) - d_{11}\,f_7(y,t) + d_{11}\,f_9(y,t) - d_{16}\,f_{10}(y,t) - d_{14}f_{11}(y,t) - d_{15}f_{12}(y,t), \tag{3.2.70}$$

$$u_{cos}(y,t) = \frac{1}{2}f_1(y,t) + \frac{1}{2}f_2(y,t) + (d_{11}+d_{16})f_3(y,t) + d_{14}f_4(y,t) - d_{11}f_5(y,t) + d_{15}f_6(y,t) - d_{11}\,f_7(y,t) + d_{11}\,f_9(y,t) - d_{16}\,f_{10}(y,t) - d_{14}f_{11}(y,t) - d_{15}f_{12}(y,t), \tag{3.2.71}$$

Here $u_{sin}(y,t)\ and\ u_{cos}(y,t)$ are the velocity profiles for sin and cosine oscillations respectively.

### 3.2.5 Nusselt Number

Using the equation (3.2.64), Nusselt number for Ramped wall temperature is

$$N_u = -[h_8(t) - h_8(t-1)H(t-1)]. \tag{3.2.72}$$

Using the equation (3.2.69), Nusselt number for Isothermal temperature is

$$N_u = -[h_7(t)]. \tag{3.2.73}$$

### 3.2.6 Sherwood Number

Using the equation (3.2.65), Sherwood Number is

$$s_h = -[h_{11}(t)]. \tag{3.2.74}$$

### 3.2.7 Skin Friction

Expressions of skin-friction for both cases are calculated from Equations. (3.2.66-3.2.67) and (3.2.69-3.2.70) using the relation

$$C_f{}^*(y,t) = -\mu_B\left(1+\frac{1}{\gamma}\right)C_f. \tag{3.2.75}$$

### 3.2.7.1 For ramped wall temperature

$$C_{f_{sin}}(y,t) = \frac{i}{2}h_1(t) - \frac{i}{2}h_2(t) + h_{13}(t) - h_{13}(t-1)H(t-1) + h_{14}(t) + h_{15}(t) +$$

$$h_{15}(t-1)H(t-1) + h_5(t) - h_{16}(t), \tag{3.2.76}$$

$$C_{f_{cos}}(y,t) = \frac{1}{2}h_1(t) + \frac{1}{2}h_2(t) + h_{13}(t) - h_{13}(t-1)H(t-1) + h_{14}(t) + h_{15}(t) +$$

$$h_{15}(t-1)H(t-1) + h_5(t) - h_{16}(t). \tag{3.2.77}$$

### 3.2.7.2 For isothermal temperature

$$C_{f_{sin}}(y,t) = \frac{i}{2}h_1(t) - \frac{i}{2}h_2(t) + (d_{11}+d_{16})h_3(t) + d_{14}h_4(t) - d_{11}h_5(t) + d_{15}h_6(t) -$$

$$d_{11}h_7(t) + d_{11}h_9(t) - d_{16}h_{10}(t) - d_{14}h_{11}(t) - d_{15}h_{12}(t), \tag{3.2.78}$$

$$C_{f_{cos}}(y,t) = \frac{1}{2}h_1(t) + \frac{1}{2}h_2(t) + (d_{11}+d_{16})h_3(t) + d_{14}h_4(t) - d_{11}h_5(t) + d_{15}h_6(t) -$$

$$d_{11}h_7(t) + d_{11}h_9(t) - d_{16}h_{10}(t) - d_{14}h_{11}(t) - d_{15}h_{12}(t). \tag{3.2.79}$$

## 3.2.8 Results and Discussion

To understand the physics of the problem, the obtained analytical solutions are studied numerically and are elucidated with the help of graphs. Parametric study is performed for Casson parameter $\gamma$, magnetic parameter $M$, Schimdt number $Sc$, permeability of porous medium $\kappa$, phase angle $\omega t$, volume fraction parameter $\emptyset$ and radiation parameter Nr in Figure 3.2.2 to Figure 3.2.10. Numerical values of skin-friction, Nusselt number and Sherwood number are computed and presented in tables for different parameters. It is evident from Figure 3.2.2 that velocity increases with decrease in volume fraction parameter $\emptyset$. Figure 3.2.3 depicts that velocity decreases with increasing values of Casson nanofluid parameter $\gamma$ for $\omega t = \pi$ and otherwise for $\omega t = 0$. Increase in Casson parameter shortens the velocity boundary layer thickness. It is observed that the non-Newtonian behavior disappears and the nanofluid behaves like a Newtonian nanofluid for sufficiently large values of $\gamma$.

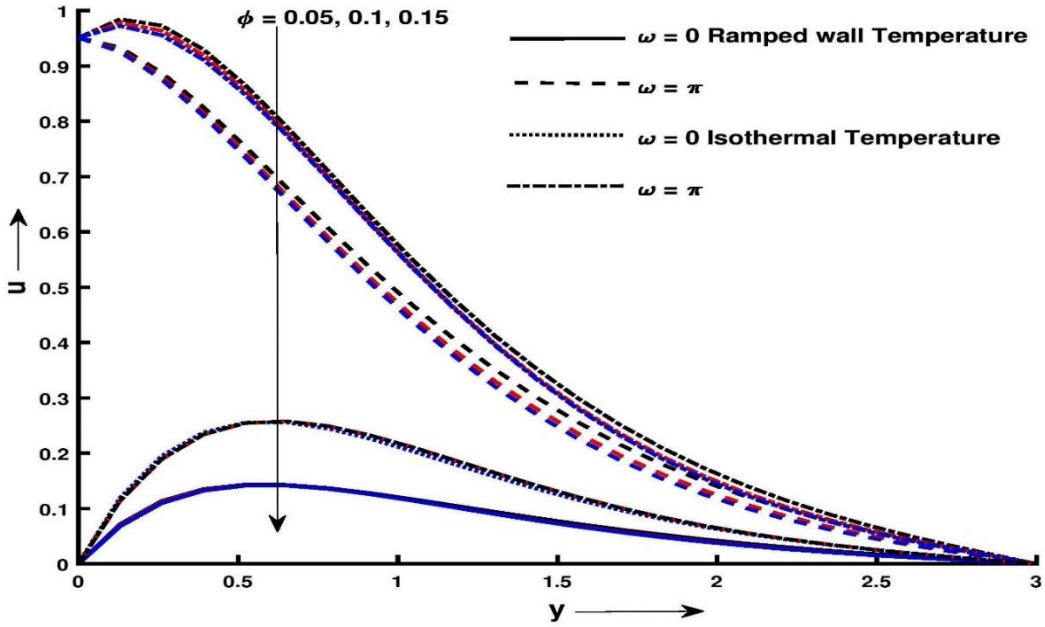


**Figure 3.2.2:** Velocity profile for $y$ and $\emptyset$ at $\gamma = 0.6,\ \kappa = 0.4, Sc = 0.5,$ $Gm = 4,\ t = 0.6,\ M = 3, Gr = 8,\ Nr = 5\ and\ Pr = 6.2$

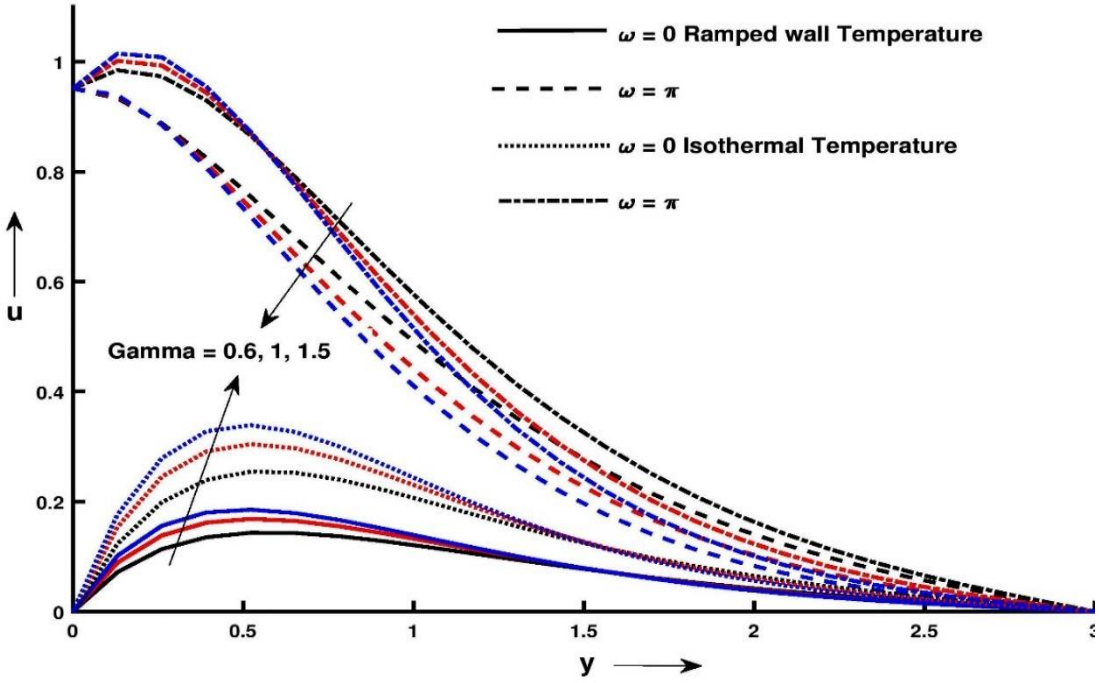


**Figure 3.2.3:** Velocity profile u for y and γ at $\kappa = 0.4, \mathrm{Sc} = 0.5,$ $\mathrm{Gm} = 4,\ \mathrm{t} = 0.6,\ \mathrm{M} = 3, \mathrm{Gr} = 8,\ \emptyset = 0.02,\ \mathrm{Nr} = 5$ and $\mathrm{Pr} = 6.2$

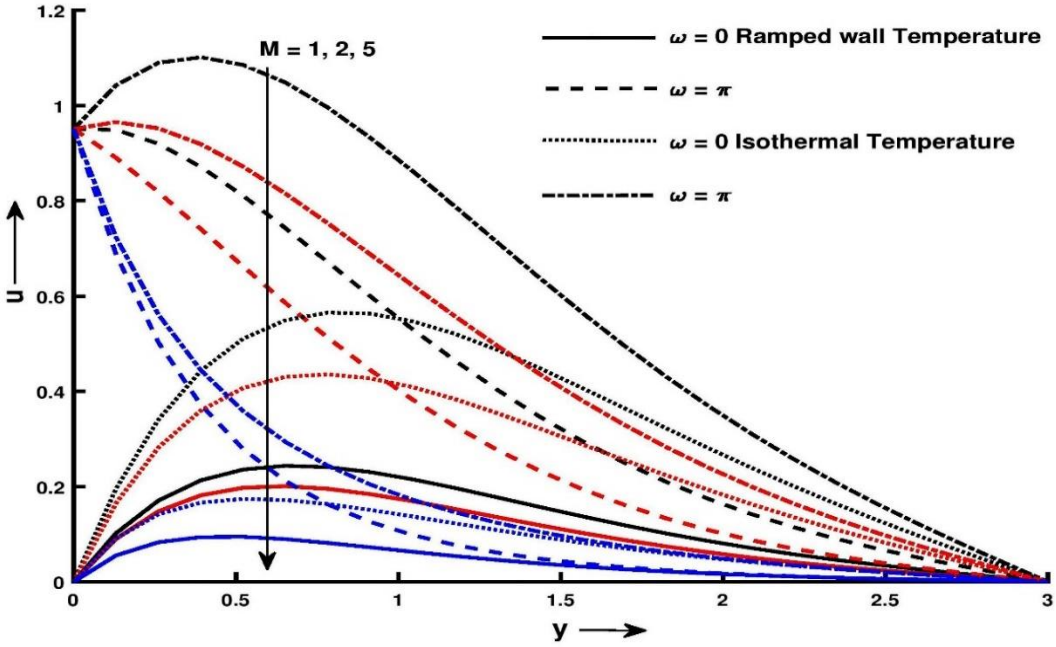


**Figure 3.2.4:** Velocity profile $u$ for $y$ and M at $\gamma = 0.6,\ \kappa = 0.4, Sc = 0.5,$ $Gm = 4,\ t = 1,\ Gr = 8,\ \emptyset = 0.02,\ Nr = 5\ and\ Pr = 6.2.$

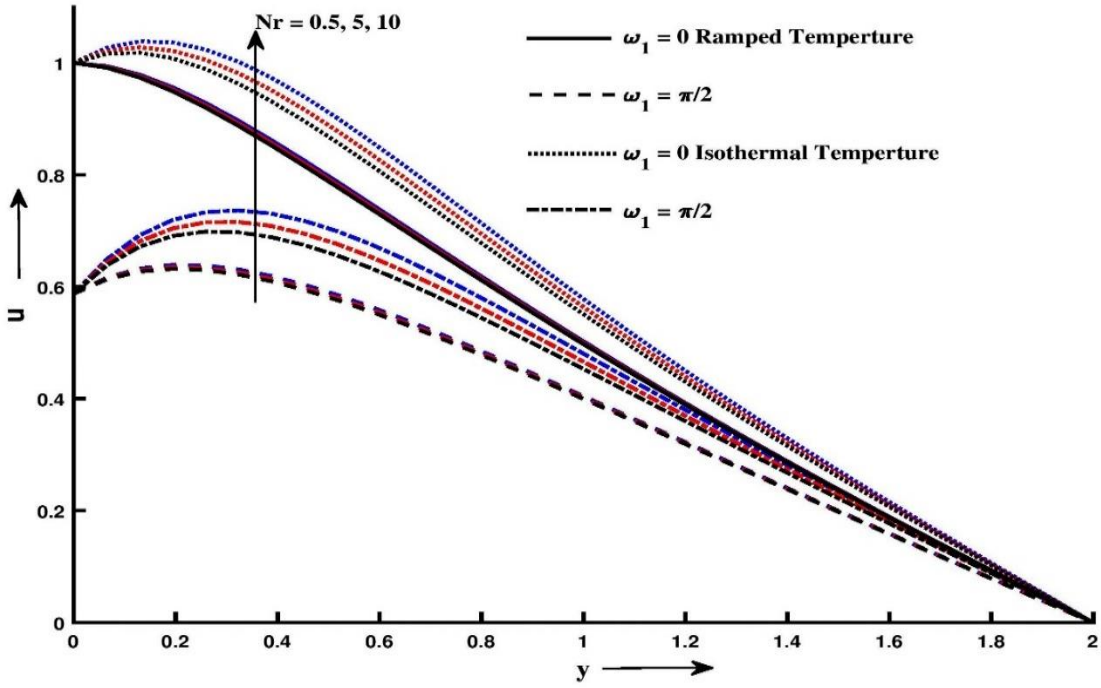


**Figure 3.2.5:** Velocity profile $u$ for $y$ and $Nr$ at $\gamma = 0.6,\ \kappa = 0.4, Sc = 0.5,$ $Gm = 4,\ t = 0.6,\ M = 3, Gr = 8,\ \emptyset = 0.02\ and\ Pr = 6.2$

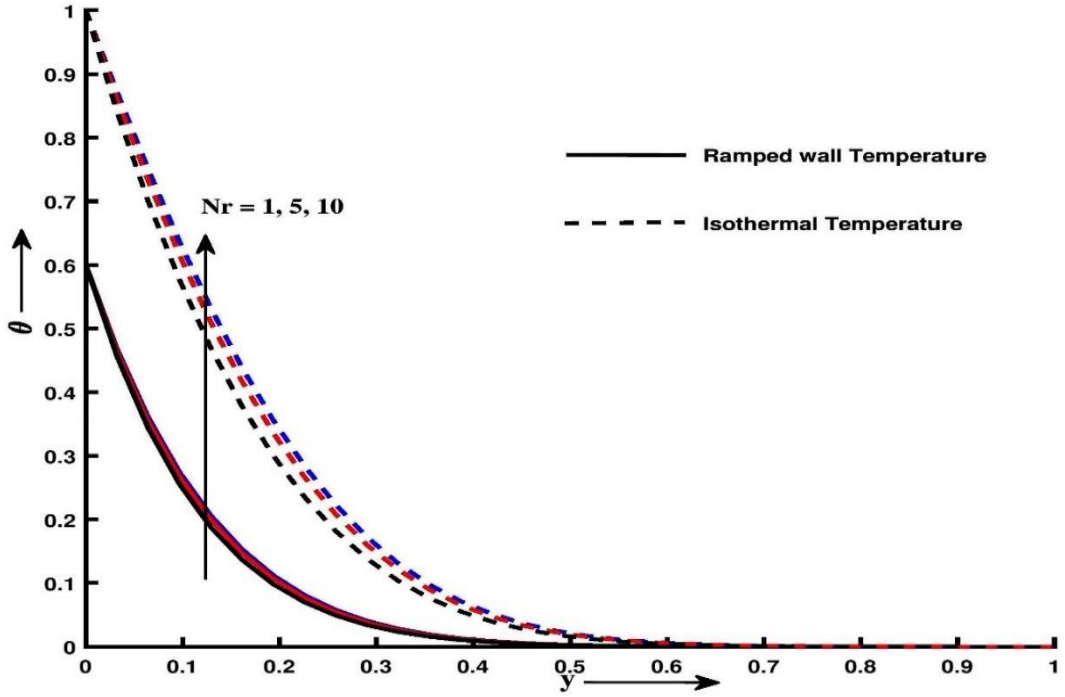


**Figure 3.2.6:** Temperature profile for $y$ and $Nr$ at $\gamma = 0.6,\ \kappa = 0.4, Sc = 0.5,$ $Gm = 4,\ t = 0.6,\ M = 3, Gr = 8,\ \emptyset = 0.02\ and\ Pr = 6.2$

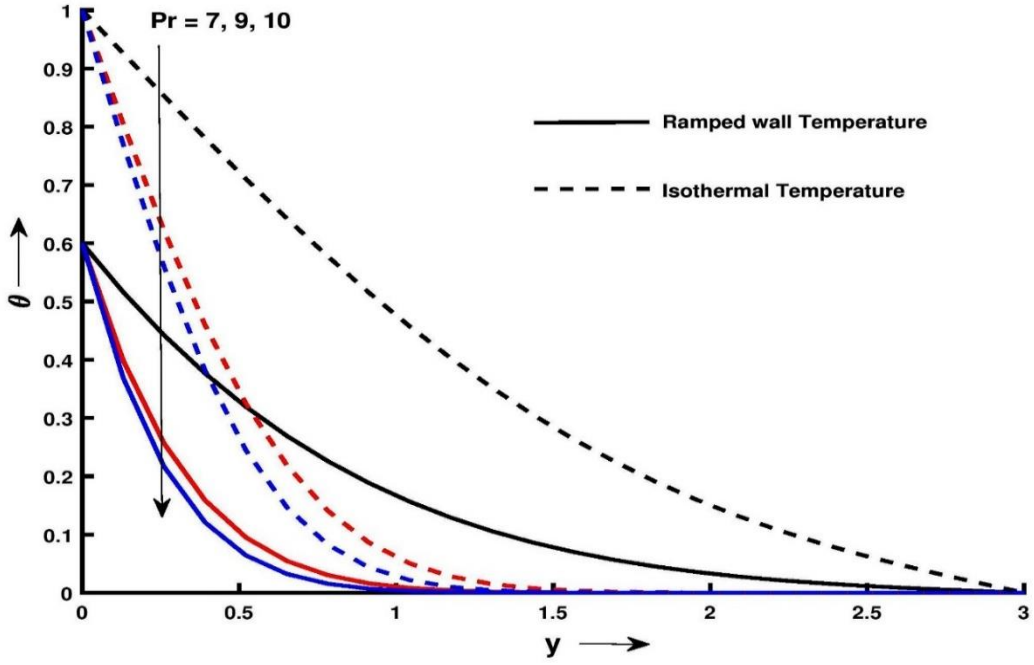


**Figure 3.2.7:** Temperature profile $\theta$ for $y$ and $Pr$ at $\gamma = 0.6, \kappa = 0.4,$ $Sc = 0.5, Gm = 4,\ t = 0.6,\ M = 3, Gr = 8,\ \emptyset = 0.02\ and\ Nr = 5.$

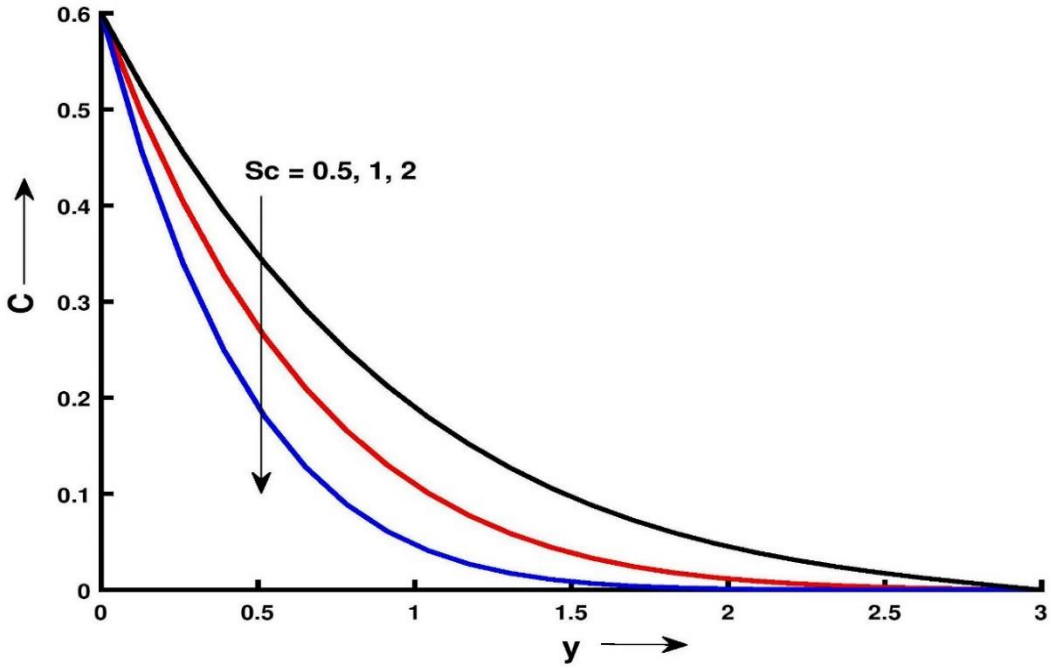


**Figure 3.2.8:** Concentration profile $C$ for $y$ and $Sc$ at $\gamma = 0.6, \kappa = 0.4$, $Gm = 4,\ t = 0.6,\ M = 3, Gr = 8,\ \emptyset = 0.02,\ Nr = 5\ and\ Pr = 6.2.$

.

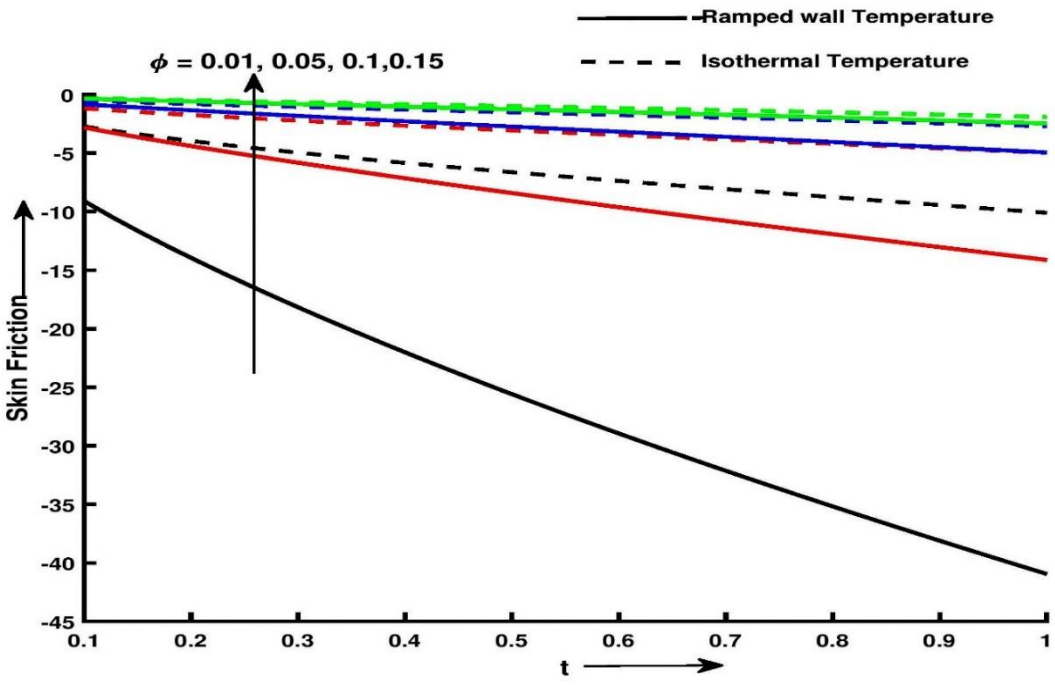


**Figure 3.2.9:** Skin Friction for $\emptyset$ and $t$ at $\gamma = 0.6,\ \kappa = 0.4, Sc = 0.5,$ $Gm = 4, M = 3, Gr = 8, Nr = 5\ and\ Pr = 6.2$

.

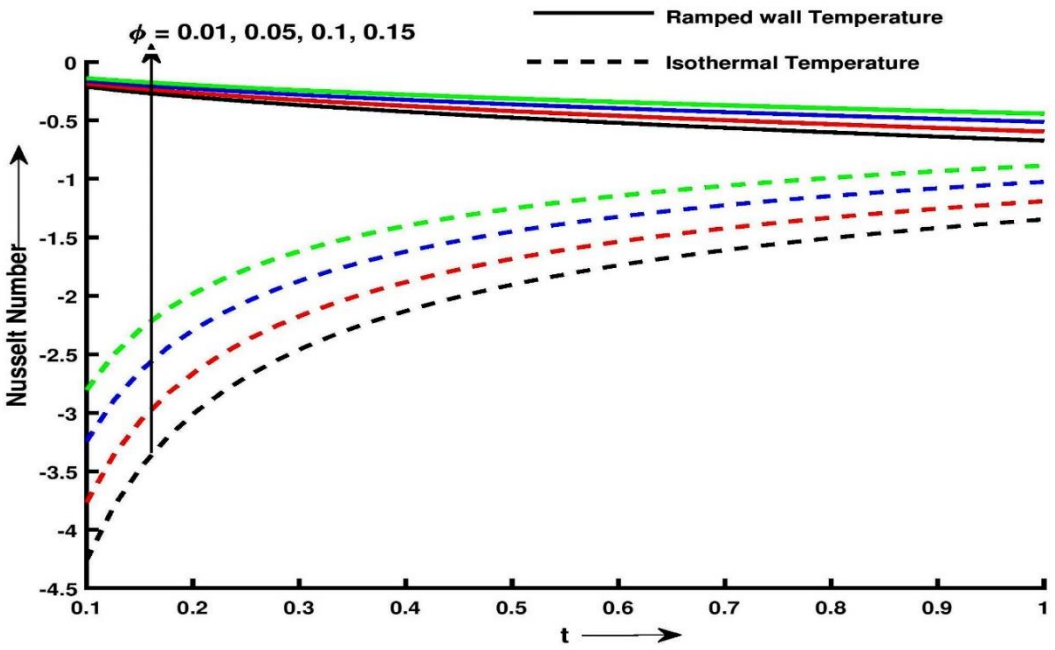


**Figure 3.2.10:** Nusselt number for $\emptyset$ and $t$ at $\gamma = 0.6,\ \kappa = 0.4, Sc = 0.5,$ $Gm = 4,\ M = 3, Gr = 8,\ \emptyset = 0.02,\ Nr = 5\ and\ Pr = 6.2$

Figure 3.2.4 shows that the nanofluid velocity diminish with increase in magnetic parameter $M$. Impact of $Nr$ and $\omega$ on the velocity is shown in Figure 3.2.5. It is evident that the fluid velocity increases with $Nr$ for different values of $\omega$. Figure 3.2.6 illustrates that there is increase in temperature with increase in radiation parameter $Nr$. Increase in $Nr$ signifies the release of heat energy into the flow region and so the fluid temperature increases. It is observed from Figure 3.2.7 that the nanofluid temperature decreases as $Pr$ increases. It is justified as thermal conductivity of nanofluid decreases with increasing Prandtl number $Pr$. It is illustrated from Figure 3.2.8, that concentration decreases on increasing $Sc$ for both cases (ramped and isothermal plates). With increase in $Sc$, the viscous boundary layer becomes relatively thicker than concentration boundary layer. As a result of greater concentration gradient, mass flux increases. Figure 3.2.9 and Figure 3.2.10 depict that both Skin friction and Nusselt number $Nu$ increase with increase in volume fraction $\emptyset$. The

numerical values of skin friction $C_f$, Nusselt number $Nu$ and Sherwood number $Sh$ are exhibited in tabular form through Tables 3.2.1 to Tables 3.2.3.

It is observed from Table 3.2.1 that, for both temperature cases, skin friction decreases with the progress of time. Skin friction is disliked in most of the technical applications. It is observed that increase in any one of the parameters $Gr, Gm, Sc$ or $\kappa$ decreases skin friction whereas increases with Casson parameter $\gamma$. It is revealed from Table 3.2.2 that, $Nu$ decreases with increase in $t$ for ramped temperature and otherwise for isothermal case. It is found from Table 3.2.3 that, Sherwood number $Sh$ decreases with increase in $t$ or Schimdt number $Sc$.

**Table 3.2.1:** Skin friction variation

| $t$ | $\gamma$ | $Sc$ | $Gr$ | $Gm$ | $\kappa$ | Skin friction $C_f$ or Ramped temperature | Skin friction $C_f$ for isothermal temperature |
|---|---|---|---|---|---|---|---|
| 0.2 | 2 | 3 | 1 | 2 | 0.4 | -0.5963 | -0.4916 |
| 0.2 | 2.1 | 3 | 1 | 2 | 0.4 | -0.5739 | -0.4780 |
| 0.2 | 2.2 | 3 | 1 | 2 | 0.4 | -0.5541 | -0.4658 |
| 0.2 | 2 | 3.1 | 1 | 2 | 0.4 | -0.6564 | -0.5517 |
| 0.2 | 2 | 3.2 | 1 | 2 | 0.4 | -0.7218 | -0.6171 |
| 0.2 | 2 | 3 | 1.1 | 2 | 0.4 | -0.6170 | -0.5018 |
| 0.2 | 2 | 3 | 1.2 | 2 | 0.4 | -0.6378 | -0.5121 |
| 0.2 | 2 | 3 | 1 | 2.1 | 0.4 | -0.6157 | -0.5110 |
| 0.2 | 2 | 3 | 1 | 2.2 | 0.4 | -0.6352 | -0.5304 |
| 0.2 | 2 | 3 | 1 | 2 | 0.5 | -0.8477 | -0.6788 |

| | | | | | | | |
|---|---|---|---|---|---|---|---|
| 0.2 | 2 | 3 | 1 | 2 | 0.6 | -1.1275 | -0.8834 |
| 0.3 | 2 | 3 | 1 | 2 | 0.4 | -0.8219 | -0.6613 |
| 0.4 | 2 | 3 | 1 | 2 | 0.4 | -1.0461 | -0.8280 |

**Table 3.2.2:** Nusselt number variation

| $t$ | **Nusselt number for Ramped Temperature** | **Nusselt number for isothermal Temperature** |
|---|---|---|
| 0.2 | -0.1982 | -1.9823 |
| 0.3 | -0.2428 | -1.6185 |
| 0.4 | -0.2803 | -1.4017 |

**Table 3.2.3:** Sherwood Number variation

| $t$ | $Sc$ | **Sherwood Number** |
|---|---|---|
| 0.2 | 3 | -0.2185 |
| 0.3 | 3 | -0.2676 |
| 0.4 | 3 | -0.3090 |
| 0.2 | 3.1 | -0.2221 |
| 0.2 | 3.2 | -0.2257 |

## 3.2.9 Conclusions

Vital remarks are summarized as follows:

- Nanofluid velocity decreases with increase in volume fraction parameter ∅.

- Velocity of the nanofluid increases with increase in radiation parameter $Nr$ for different frequencies of oscillation $\omega$ of the plate.
- Nanofluid velocity is getting decelerated with increase in magnetic parameter $M$.
- Nanofluid velocity is more for $\omega t = \pi$ than $\omega t = 0$.
- Nanofluid velocity is more for isothermal temperature compared to ramped plate.
- Temperature of nanofluid increases with increase in the radiation parameter $Nr$.
- Nanofluid temperature decreases with rise in values of Prandtl number $Pr$.
- Concentration tends to decrease with increase in Schimdt number $Sc$.
- Nusselt number $Nu$ increases with time $t$ for isothermal case and otherwise for ramped temperature case.
- Sherwood number $Sh$ decreases with increase in $t$ or Schimdt number $Sc$ for both ramped temperature and isothermal plate.